THE JOURNAL OF PHYSICAL CHEMISTRY Letters

Letter

pubs.acs.org/JPCL

Countercations Control Local Specific Bonding Interactions and Nucleation Mechanisms in Concentrated Water-in-Salt Solutions

Hsiu-Wen Wang,*[,†] Trent R. Graham,[‡] Eugene Mamontov,[§] Katharine Page,[§] Andrew G. Stack,[†] and Carolyn I. Pearce[‡]

[†]Chemical Sciences Division and [§]Neutron Scattering Division, Oak Ridge National Laboratory, Oak Ridge, Tennessee 37831, United States

[‡]Pacific Northwest National Laboratory, Richland, Washington 99352, United States

Supporting Information

ABSTRACT: One of the continuing challenges presented in salt solutions is understanding ion association reactions driving dynamic demixing from solvation, complexation, and solute clustering. The problems understanding this phenomenon are exacerbated in the highly concentrated water-in-salt solutions, where the deficiency of water leads to a dramatic retardation of water solvent and formation of extended solvent−solute clustering networks. By probing microscopic dynamics of water and prenucleation clusters using quasi-elastic neutron scattering and proton nuclear magnetic resonance spectroscopy, we observed contrasting mechanistic specifics of ion−water mobilities in highly concentrated Na^+- versus K^+-based aluminate solutions (diffusion coefficients of 0.2 vs 2.6 × 10^{-10} m^2 s^{-1} at 293 K, respectively). The magnitude of the differences is far beyond countercations acting as simple innocent charge-balancing species or water solvents functioning as a simple medium for ion diffusion. The distinct crystallization mechanisms observed further imply that different prenucleation cluster dynamics can either frustrate or promote crystallization, as described by nonclassical nucleation theory.

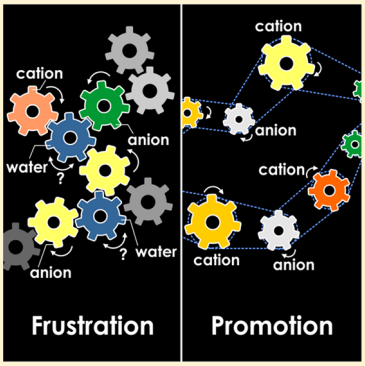

The structure and dynamics of aqueous salt solutions extended to regions of low water activity represent an increasingly important topic crossing a wide range of applications in chemical synthesis, energy storage, radioactive waste remediation, and industrially relevant processes. Introducing a few moles of water per mole of Li^+TFSI^- electrolytes, for instance, can break apart aggregates of ions and facilitate Li^+ migration, while maintaining the desirable voltage window in Li-ion batteries.[1] Rate-limiting reactions for nucleation of crystals from salt solutions have been linked to formation of ion-association complexes[2−7] or from prenucleation clusters presented as highly charge ions through nonclassical nucleation mechanisms with underlying complex ion−water interactions.[7−10] In the past decade, the existing textbook knowledge on solution-phase interactions and homogeneous nucleation mechanisms have been continuously challenged. For example, Widmer and Schwartz[11] demonstrate a concept of solvents partnering with a solute in solution to form stable chemically distinct molecular identities, which control the associated reactions beyond the typical view of solvents as a simple medium that allows the reactants to interact via diffusion. A parallel concept is also proposed for the role of counterions in solution chemistry, where the presence of multiple dissolved solutes sets up a competition for water molecules and can control solute molecular speciation beyond their innocent charge-balancing roles. In fact, many steps in chemical synthesis make use of counterions' properties to mediate rates of reactant encounters[12,13] and control specific solid-phase formation.[3] Furthermore, arguments about the thermodynamics of solvated chemical species have triggered a growing body of literature arguing for nonclassical mechanisms of nucleation that include prenucleation cluster formation.[6,8−10,14] In their most recent article, Gebauer and Wolf[14] assess the current needs for fundamental understanding of highly dynamic oligomeric/polymeric solute entities to map out a new comprehensive picture for the design of chemical synthesis with targeted structures.

In addition to these recent emphases, the traditional view in dilute solutions that ions are differentiated as being kosmotropes or chaotropes based on their ability to increase or decrease water structuring or the viscosity of water[15−18] is no longer valid in "water-in-salt" scenarios, simply because of the crowding of water and molecular ions at high salt concentrations. Geometric frustration, in which molecules have the potential to assume a packing that locally minimizes enthalpy but frustrates crystal nucleation is another important factor affecting nucleation in high salt solutions.[4] Frustration (against crystallization) through formation of locally favored structures is believed to play a crucial role in glass formation processes in supercooled water and in some metallic glass formers.[19−21] The disruption of water−water tetrahedral structuring by local ion−water and ion−ion complexations

Received: May 17, 2019
Accepted: May 30, 2019
Published: May 30, 2019

DOI: 10.1021/acs.jpclett.9b01416
J. Phys. Chem. Lett. XXXX, XXX, XXX−XXX

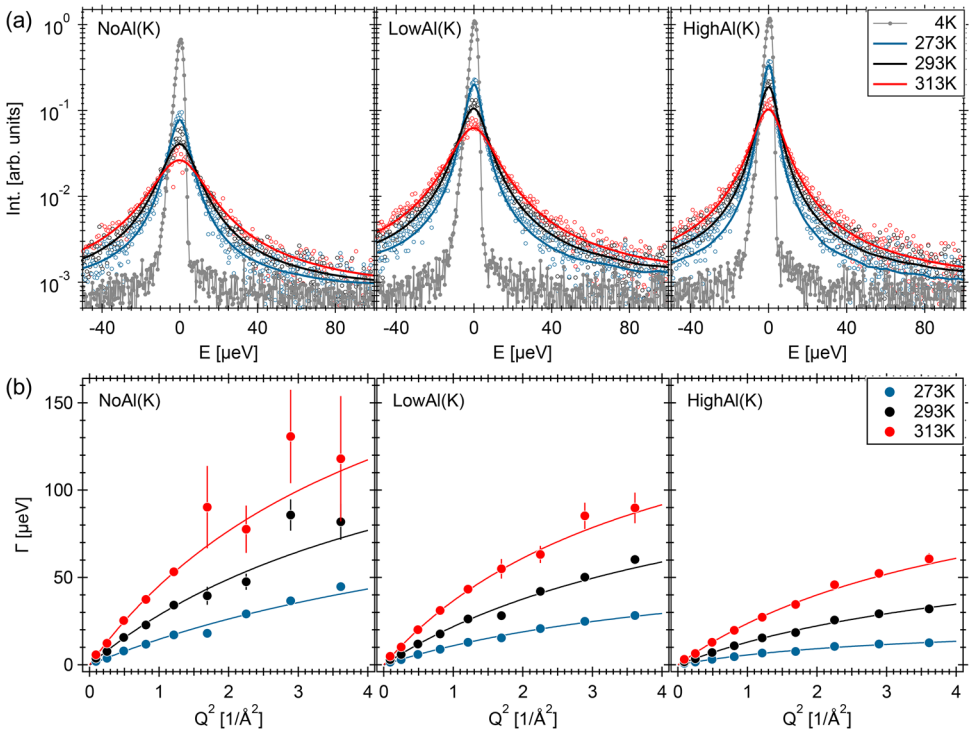

Figure 1. QENS spectra and analysis for concentrated KOH (NoAl) and potassium aluminate solutions (LowAl and HighAl) at different temperatures and at $Q = 0.5$ Å^{-1}. The spectra in gray correspond to the experimental resolution function. The color dots represent the experimental spectra, while the solid lines represent the fitting curve (*individual* Q-dependent fit) using one Lorentzian scattering function. See the Supporting Information for fitting details. (b) Q^2-dependence of HWHM of the Lorentzian component $\Gamma(Q)$ (color circles) obtained from the QENS data fits. The solid lines are the fits of the HWHM with a jump diffusion model using eq 1.

results in dynamic and structural heterogeneities leading to the behaviors of concentrated salt solutions reminiscent of supercooled liquids approaching the glass transition.[22,23]

Highly concentrated alkaline aluminate solutions are a relevant example that can easily reach high levels of supersaturation and remain metastable at room temperature for weeks without crystallization.[24] Concentrated aluminate solutions, particularly sodium aluminate, sodium hydroxide, and other highly soluble salts, are the dominant chemical components of high-level radioactive waste liquids at the Hanford Site, Hanford, WA. Remediation of high-level nuclear wastes resulting from Cold War activities at Hanford is one of the greatest challenges for DOE's Office of Environmental Management.[25,26] The highly charged Al^{3+} cations easily undergo hydrolysis under acidic or alkaline conditions, forming various aqueous hydroxylated Al^{3+} species.[27] Multiple possible Al (oxy)hydroxide phases can be precipitated depending on the aluminum speciation in solution.[28,29] In basic solutions, where the aluminate anion ($Al(OH)_4^-$) is the dominant hydrolytic species, gibbsite ($Al(OH)_3$) or boehmite (AlOOH) are the phases that typically precipitate through ion aggregations, involving aluminate monomers or coalesced polynuclear species together with alkali-metal cations.[24,29−31] The presence of countercations (e.g., Na^+ or K^+) is thought to play an essential role in stabilizing a network of aluminate ion pairs and controlling the consequent aggregation behavior.[24,30−32] However, the direct influence of countercations on speciation equilibria and stabilization of polynuclear aluminate complexes is poorly understood. This is particularly true at high alkalinity, where the excess caustic species (NaOH or KOH) increase aluminate solubility and move the equilibria from gibbsite (or boehmite)-controlled solubility to solubility controlled by hydrous (or anhydrous) salts of alkaline aluminates.[24,25,33−38]

Herein we combine quasi-elastic neutron scattering (QENS) and proton, pulsed field gradient, nuclear magnetic resonance spectroscopy (^{1}H PFG-NMR, in short NMR) to characterize the spatial and temporal dynamics of KOH−$KAl(OH)_4$−H_2O compounds at very high ionic concentrations. To understand the interactions between aluminate complexes and alkali-metal cations presented in solution and how these interactions affect nucleation behaviors at high concentrations, we specifically investigate K^+-based aluminate solutions at an ionic concentration identical to that in our previous QENS/NMR work on Na^+-based aluminate solutions.[39] These two aluminate solution systems differ only in counteraction selection (Na^+ vs K^+; Table S1 in the Supporting Information). We find that the choice of countercations influences aluminate polymerization and the network morphology of aggregated ion clusters, which affect ion−water mobility far beyond the kosmotropic (Na^+) and chaotropic (K^+) effects typically observed at low ionic concentrations. Furthermore, we show that the distinct crystallization mechanisms observed in Na^+ versus K^+-based solutions are correlated with different cluster dynamics and suggest that the concept of nonclassical mechanisms of nucleation can be tailored with the control of solute molecular reactions.

Given that the structural changes in aqueous solutions have strong effects on dynamics, the motions of H-bearing species (OH^-, H_2O, $Al(OH)_4^-$, and Al-clusters) obtained in a broad range of time scales (QENS and NMR) contain rich information on the underlying local specific interactions responsible for distinct solute−water clustering dynamics in the concentrated/condensed aqueous system. Hereafter, and

DOI: 10.1021/acs.jpclett.9b01416
J. Phys. Chem. Lett. XXXX, XXX, XXX−XXX

throughout the rest of this Letter, we follow our previous notation[39] and refer to three K^+-based solutions as NoAl(K) for the 20 m aluminum-free KOH solution and LowAl(K) and HighAl(K) for the two potassium aluminate solutions with 5.9 and 9.5 m total aluminum, respectively (Table S1). Note that the mole ratio of $K^+/Al(OH)_4^-$ = 3 in LowAl(K) and HighAl(K) solutions is equivalent, and they differ only by the degree of dilution. At the same ionic concentration, Na^+-based solutions are always more viscous than solutions containing K^+, and the viscosities are increasingly enhanced with the presence of aluminate in Na^+-based solutions,[40−42] reflecting a greater solution structure-making ability in the presence of Na^+.

The temperature-dependent QENS spectra (at $Q = 0.5$ Å^{-1}) of the three solutions are shown in Figure 1a. They feature a systematic line width broadening with increasing temperatures or decreasing concentrations, indicating that species are more mobile under these conditions. In contrast to our previous QENS study of Na^+-based solutions, the observed QENS broadening is adequately described with using only one Lorentzian scattering function to fit the data independently at each Q value (as *individual* Q-dependent fit; Supporting Information 2). The Q-dependence of Lorentzian fit component broadening $\Gamma(Q)$ (half-width at half-maximum, HWHM) presented in Figure S1 follows the power law relationship, $\Gamma(Q) = \Gamma^o Q^\lambda$, with the slope λ slightly below 2 (λ = 2 represents standard Brownian diffusion). Alternatively, the well-known jump diffusion model is adopted to illustrate the Q-dependence of the diffusion processes involved (Figure 1b). The expression for the Singwi−Sjölander jump diffusion model (eq 1) is[43]

$$\Gamma(Q) = \frac{\hbar}{\tau_{jd}}\left[1 - \frac{1}{1 + DQ^2\tau_{jd}}\right] \quad (1)$$

Here, $\hbar$ is the reduced Planck's constant and τ_{jd} is the residence time between the jumps of a diffusing molecule (center of mass) with a long-range translational diffusion coefficient $D = \langle l^2\rangle/6\tau_{jd}$, where $\langle l^2\rangle^{1/2}$ is the apparent mean-square jump length. The error bars on data for the NoAl(K) solution (pure 20 m KOH) at 313 K are sizable at high Q values, because the line width becomes comparable to the dynamic range of the instrument (Figure 1b). Overall, all K^+-based solutions show an initial linear region following $\Gamma(Q \rightarrow 0) = \hbar DQ^2$ and then a gradual flattening out to an approximately constant valve given by $\Gamma(Q\rightarrow\infty) = \hbar/\tau_{jd}$, which are characteristic of jump diffusion processes. We also applied a *global* Q-dependent fit with jump diffusion expression directly (Supporting Information 2), in which τ_{jd} and D are the fit parameters that characterize the line width for all Q values (as a *global* feature) at each measured temperature. The QENS spectra obtained in our analyses thus represent motions of H-bearing species in the accessible time window of the spectrometer (~6−400 ps, determined by its energy resolution) and reflect the averaged diffusion of these species.

Figure 2 displays the derived diffusion coefficients (D) of the three studied K^+-based solutions compared with (i) pure water[19,44,45] and (ii) Na^+-based solutions.[39] The D value for bulk water is ~20.3−22.2 × 10^{-10} m^2/s at 293 K.[19,44,45] Within a temperature range of 273−353 K, the QENS-derived D values for the concentrated K^+-based solutions are approximately consistent with NMR results (Figure 2; see Supporting Information 3 for NMR analysis). The diffusivity decreased by

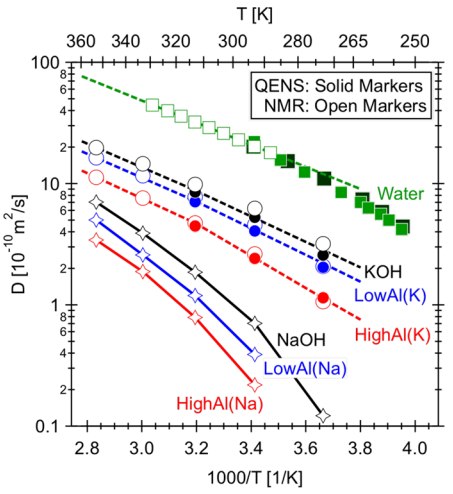

Figure 2. Temperature dependence of the diffusion coefficients in concentrated KOH and potassium aluminate solutions measured using QENS and NMR. Diffusion coefficients for solutions containing Na^+ are from Graham et al.[39] Data for bulk water[19,44,45] is also shown for comparison. The Arrhenius fits (dashed lines) yield activation energies, which are summarized in Tables S2 and S3. Error bars are smaller than the symbols for all data points.

a factor of ~3, 5, and 8 in NoAl(K), LowAl(K), and HighAl(K) solutions, respectively, compared to bulk water diffusion at 293 K (see Tables S2 and S3 for the exact D values). In contrast, the decrease in diffusivity for Na^+-based solutions was much greater, with D values (from NMR[39]) reduced by a factor ~29, 52, and 92 in NoAl(Na), LowAl(Na), and HighAl(Na) solutions, respectively, when compared to bulk water at 293 K. Such an order-of-magnitude differences in diffusion constants between K^+- and Na^+-based solutions also manifests in their temperature-dependent behavior (Figure 2). The temperature dependence of the NMR-derived D value in bulk water (>293 K) can be described by fitting the data using the Arrhenius equation to give an activation energy (E_a) of 17.4(1) kJ/mol, whereas low-temperature supercooled water is noticeably known to be super-Arrhenius.[19,44] The three K^+-based solutions show behavior close to that described by the Arrhenius equation, whereas Na^+-based solutions clearly show super-Arrhenius behaviors over the same temperature range (Figure 2). To facilitate comparison of the activation energies (which depend weakly on the temperatures in K^+-based solutions), E_a values are determined using the Arrhenius equation with segmented data points. E_a values of 18.6(2), 18.9(2), and 19.9(2) kJ/mol for NoAl(K), LowAl(K), and HighAl(K) solutions, respectively, are obtained at temperatures above 313 K (Table S3), and they increase to 21.4(2), 22.1(2), and 24.3(3) kJ/mol at temperatures below 313 K (Table S2). In contrast, E_a values are 31(1), 33(1), and 34(3) kJ/mol for NoAl(Na), LowAl(Na), and HighAl(Na) solutions, respectively, based on data points at/above 313 K (Table S3).

QENS studies of nonglass- and glass-forming liquids, Ga and Se, respectively, have shown a single jump-diffusion process in Ga, whereas in Se there is a spatially localized (faster) process which requires a two-Lorentzian model fit.[46] Here we observed a similar trend in high salt solution systems. The two-Lorentzian model that is required to fit data for highly viscous Na^+-based solutions yields a spatially localized (faster) dynamic process (with almost no Q-dependence) for the broad component and a slow collective diffusion for the

DOI: 10.1021/acs.jpclett.9b01416
J. Phys. Chem. Lett. XXXX, XXX, XXX−XXX

narrow components.[39] Microscopically, we relate this observation to the presence of an extended solvent-shared-solute clustering network or "caging" effects influencing local structure in Na^+-based solutions. This prolongs the residence time between successive diffusion jumps and significantly hampers the translational diffusion processes, as evidenced by the temperature dependence of the diffusion coefficients and activation energies discussed above. In contrast, the one-Lorentzian model appropriate for less viscous K^+-based solutions, its broadening Q-dependence (approached zero in the low Q-limit as shown in Figure 1b), and the derived diffusion coefficients (Figure 2), all suggest a much weaker caging capability (or a stronger network-breaking effect) and a consequent faster diffusive motion from the solutions containing K^+.

Although QENS is limited in resolving the dynamic details of individual H-bearing species in the studied solution system, there must be a microscopic mechanism beyond the dictum that Na^+ is a kosmotrope and K^+ is a chaotrope. At low salt concentrations (salt-in-water), QENS studies of NaCl and KCl salt solutions (at 295K) revealed a slowing down of the diffusive motion of water molecules surrounding Na^+ (D = ~19.5 × 10^{-10} m^2/s for 1 M NaCl) but a slight speeding up of this diffusive motion for water around K^+ (D = ~21.3 × 10^{-10} m^2/s for 1 M KCl).[47] NMR measurements of 3 M NaOH and KOH solutions (at 295 K, in the presence of 0.1 M $Al(OH)_4^-$) indicate much reduced proton motions in NaOH solution (D = ~12.5 × 10^{-10} m^2/s) as compared to KOH solution (D = ~18.4 × 10^{-10} m^2/s) at the same ionic concentration.[48] These observed differences in diffusivity are in general correlated to the altered water hydrogen-bonding network influenced by the cations, where K^+ significantly disrupts the water network geometry and leaves a larger free volume for the faster diffusion in their vicinity. As the salt concentration increases, the degree of ion association in aqueous solution has significant effects on both the equilibrium (e.g., activity coefficients, solubility, and structure of precipitated phases) and transport properties (e.g., viscosity, diffusion coefficients, and conductivities). The law of matching water affinities, proposed by Collins et al.,[15,16] qualitatively rationalizes specific-ion pairing behaviors and illustrates that ion hydration−dehydration (solvation−desolvation) should be the dominate force impacting on the type of ion pairs (contact or solvent-shared/separated ion pairs) that forms in the salt solution. However, examples[3,49] have shown that this simple law cannot describe ion interactions in complex salt solutions, such as solutions containing multiple solutes and complex ions like oxyanions or carboxylate ions. In highly concentrated potassium- and sodium-aluminate-hydroxide solutions (water-in-salt), the deficiency of water molecules leads to the extended connectivity of ion−ion and ion−water networks simply based on geometric (packing) effects alone. This incurs a scenario that packing of molecular ions and network morphologies, as a result of coordinating ionic radii, charges, geometry, and hydrogen bonding, should be another factor (in addition to ion hydration−dehydration) for the distinct diffusive properties observed in QENS and NMR spectroscopy data. Additionally, ion aggregation behaviors in high salt solutions also directly relate to the conformational stability and the mechanisms underlying how these solutions can exist at supersaturated conditions for extended periods of time.

We hypothesize that the identities of counteractions (K^+ vs Na^+) in the studied solutions control the local specific interactions responsible for distinct solute−water clustering dynamics and lead to a contrast nucleation behavior in these highly concentrated solution systems. Evidences to support this statement is discussed below. First, the existing Car−Parrinello molecular dynamics (CPMD) calculations for ~19 m NaOH and KOH solutions imply cation-dependent hydroxide−water complex formation, with the occurrence of $OH^-(H_2O)_3$ complexes increased by the direct contact of OH^- with K^+, and Na^+ stabilizing the $OH^-(H_2O)_5$ complex by forming solvent-shared ion pairs.[50] The size of Na^+ and its octahedral coordination with water are particularly compatible with the size/geometry of the $OH^-(H_2O)_5$ complex, as demonstrated in these CPMD simulations.[50] The formation of solvent-shared ion pairs between Na^+ and OH^- at high concentrations is further supported by the recent experimental radial distribution function analyses[51] and their agreement with various classical MD models, particularly with density functional theory (DFT)-based reactive high-dimensional neural network (HDNN) potentials.[52] The preferential stabilization of specific hydroxide−water complexes by countercations does not appear to be limited to the simple hydroxide solutions (see examples in ref 3). As the solution concentration of aluminum increases in high alkalinity, dimeric species (e.g., $[Al_2(OH)_8]^{2-}$ or $[Al_2O(OH)_6]^{2-}$) form in competition with aluminate $Al(OH)_4^-$ monomers. The molecular constituent, structure, and stability of these polynuclear complexes are highly influenced by the nature of countercation because of cation−anion interactions. For instance, early DFT studies predicted that the solvent-shared ion pairing between Na^+ and $Al(OH)_4^-$ is energetically more favorable than the formation of contact ion pairs, because the shared water molecule renders its properties so that they are similar to the isolated ions.[53] Other ab initio molecular dynamic (AIMD) simulations of the dimeric aluminate species reveal that, in the absence ion pair formation, the hydrated $[Al_2(OH)_8]^{2-}$ dimer is energetically more stable than the $[Al_2O(OH)_6]^{2-}$ dimer, but the stabilities of these two dimers are reversed when Na^+ is ion-paired with $[Al_2O(OH)_6]^{2-}$ species.[54,55]

As a gauge of the countercation's role in directing the aluminate oligomerization processes, our corresponding Raman spectra (Figure 3) indicate that the intensity of the two sidebands (at ~540 and 710 cm^{-1}), formed at the expense of $Al(OH)_4^-$ monomer (Raman signal at ~624 cm^{-1}), provide strong evidence for different aluminate speciation in the presence of Na^+ versus K^+. The intensity of the two sidebands is much more pronounced relative to $Al(OH)_4^-$ monomer from the aluminate solutions containing Na^+. Although the origin of these Raman sidebands is still a controversial topic, they have been arguably assigned to oxygen-bridged $[Al_2O(OH)_6]^{2-}$ dimer or associated with larger polynuclear species.[24,55] Raman spectra in Figure 3 do indicate that, in the presence of K^+, the formation of aluminate polymeric species in equilibrium with the monomers is suppressed. These results suggest that the weaker potassium−water hydration reactions allow K^+ to be engaged in more direct ionic interactions with $OH^-(H_2O)_3$ trihydrates than do the smaller Na^+ cation, which prefers to retain its (partial) hydration shell. The cation−anion association between $K^+/OH^-/Al(OH)_4^-$ species necessitates liquid−liquid phase separation (i.e., formation of a dense solute-rich phase and a lean region of dilute ionic solution phase) and dynamic demixing fluctuations, which are consistent with the fast diffusivity (low

DOI: 10.1021/acs.jpclett.9b01416
J. Phys. Chem. Lett. XXXX, XXX, XXX−XXX

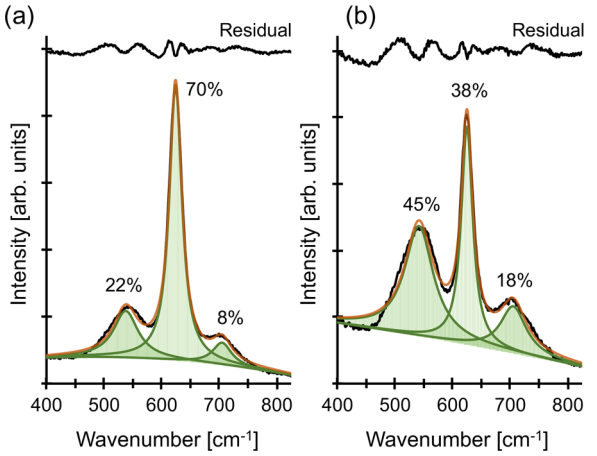

Figure 3. Room-temperature Raman spectra of LowAl solutions in the presence of (a) K^+ versus (b) Na^+ countercations. A linear background correction was applied. Al−O stretching bands at ∼540 and 710 cm^{-1}, are attributed to of higher order aluminate clusters, such as dimers. The Al−O stretching band of aluminate monomers is assigned to the band at 624 cm^{-1}. The data curve is shown in black. The fitted curve and its deconvolution components are shown in brown and green. The residual plots are given in the upper panel within each plot. See Supporting Information 4 for details on Raman measurements.

viscosity) observed in QENS and NMR data. A similar heterogeneous fluid structuring with the formation of nonionic and ionic domains was also proposed to explain rapid CO_2 diffusivity in viscous organic solvents.[56] The tendency for water solvent to be shared between Na^+/OH^- ions and the higher degree of aluminate polymerization in the sodium-aluminate-hydroxide solutions, in contrast, enhance the formation of extended solvent−solute clustering network. This network causes a stronger structural trapping effect for water molecules (e.g., H_2O bridged between Na^+ and OH^- ions) and restricts the motion of large oligomeric aluminate species (e.g., H_2O or OH^- species bridged between two distinct dimeric species and their complex introversions).

Additional evidence to support the important role that counterions play in these highly concentrated solutions is provided by the distinct nucleation and solid-phase precipitation behavior of LowAl and HighAl aluminate solutions, which are both supersaturated with respect to their corresponding crystalline phases (details are presented below). The framework of classical nucleation theory is that ion pairs and complexes in supersaturated solutions aggregate to form initially unstable nuclei until a critical size is reached. Recent work on supersaturated $CaCO_3$ solutions by Gebauer and others[8−10,14,57,58] has shown that the presence of stable prenucleation clusters, which are highly dynamics chains of alternating cations and anions (termed DOLLOP: dynamically ordered liquid-like oxyanion polymers), is well-related to the liquid−liquid separation event and the distinct dynamic changes in the water hydrogen-bonding network upon formation of dense solute droplets (as prenucleation clusters). Together, this establishes a nonclassical nucleation pathway from aggregation and solidification of precursor droplets to crystallization. We observed that, given the same ionic concentration, the nature of counteractions (K^+ or Na^+) leads to a dramatically different nucleation behavior. A white crystalline precipitate of $K_2[Al_2O(OH)_6](s)$[59] forms directly from supersaturated potassium aluminate solutions within a few hours to days at room temperature (Figure 4a,c). Sodium

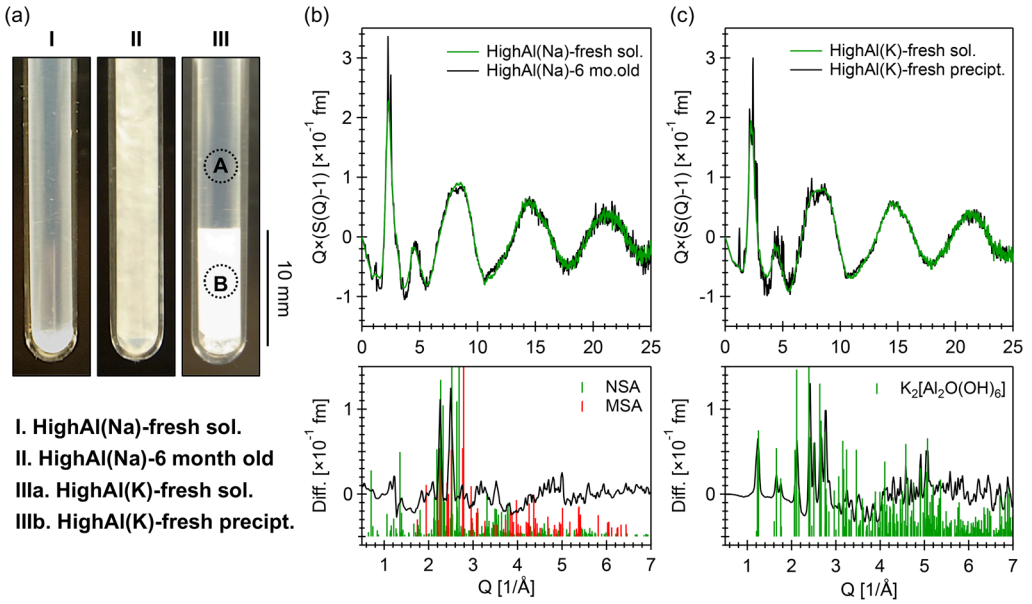

Figure 4. (a) Photographs of the deuterated HighAl(Na) (I and II) and HighAl(K) (III) solution samples taken at different times since the preparation. Show in panels b and c are the corresponding normalized neutron structure factor $S(Q)$ of the (b) HighAl(Na) and (c) HighAl(K) solutions. In panel b, measurements were performed approximately 6 months apart, and the sample photos (panel a) indicate the gelling crystallization. This data set shows the occurrence of Bragg reflections associated with NSA/MSA precipitation, and the difference of these two $S(Q)$ given in the bottom of panel a roughly matches to the calculated neutron (hkl) reflections of NSA and MSA phases. In panel c, the data set was collected on the same day, but with the precipitates forming at the bottom of the solution (see photo in panel a). The two $S(Q)$ patterns were collected with the center of neutron beam offset by ∼10 mm, as illustrated in panel a image (positions A and B). The corresponding difference pattern and the (hkl) reflections given at the bottom of panel c indicate the formation of the $K_2[Al_2O(OH)_6]$ phase. See Supporting Information 5 for details on neutron diffraction measurements and deuterated sample preparations.

DOI: 10.1021/acs.jpclett.9b01416
J. Phys. Chem. Lett. XXXX, XXX, XXX−XXX

aluminate solutions, in contrast, showed a surprising (meta)-stability and maintain a supersaturated state up to 3−6 months at room temperature. Over these long induction times, sodium aluminate solutions progressively lose fluidity and gelate into a semitransparent clot with a mixture of crystalline phases that coprecipitated during the gelling of the solutions (Figure 4a). The identifiable crystalline phases (Figure 4b) are consistent with nonasodium aluminate hydrate (NSA; also called trisodium aluminate, TSA;[34] $Na_9[Al(OH)_6]_2(OH)_3{\cdot}6H_2O_{(s)}$ = $2[Na_3Al(OH)_6]{\cdot}3NaOH{\cdot}6H_2O(s)$ = $4.5Na_2O{\cdot}Al_2O_3{\cdot}13.5H_2O$), together with a small fraction of monosodium aluminate hydrate (MSA;[33,38] $Na_2[Al_2O_3(OH)_2]{\cdot}1.5H_2O(s)$ = $Na_2O{\cdot}Al_2O_3{\cdot}2.5H_2O$). In light of formulating advanced nucleation theories, the observed precipitation behavior of these potassium and sodium aluminate solutions underpins the important role that prenucleation clusters play in the nonclassical nucleation theory. Depending on the local packing of molecular ions and the network morphology of ion−ion clusters, it appears that the prenucleation clusters can either (a) manifest themselves in densely packed arrangements that locally minimize the hydration enthalpy but frustrate the formation of the thermodynamically stable crystalline phases or (b) promote nucleation through onset of dynamic liquid−liquid separation, in which the nucleation probability would be greatly enhanced. The frustration (packing arrangement) mechanism is similar to that established for glass-forming liquids and explains the surprising metastability, high viscosity, dynamically slow ion−water motion, and gelatinous crystallization behavior in the sodium aluminate solution system. The promotion mechanism (liquid−liquid separation) follows the established view on nonclassical nucleation in supersaturated $CaCO_3$ solutions,[8−10,14,57,58] where the spatial concentration fluctuation upon liquid−liquid separation is proposed as the microscopic mechanism for the fast ion−water diffusion dynamics and precipitation kinetics observed in the potassium aluminate solution systems.

In summary, using QENS and ^{1}H PFG-NMR spectroscopy, the temperature dependence of the diffusion coefficients of H-bearing species in highly concentrated, alkaline aluminate solutions is quantified. This analysis reveals that Na^+ and K^+ metal cations partnering with water solvents introduce significantly distinct dynamics far beyond their charge-balancing roles and kosmotropic−chaotropic characters. At the studied concentrations, Na^+ preferentially enhances the formation of oligomeric aluminate species and an extended solvent-shared-solute clustering network, whereas K^+ shows stronger ion pairing effects with monomeric aluminate and hydroxide species (likely because of a smaller desolvation penalty). The nature of the alkali metal imposes distinct microscopic ion association behavior during the prenucleation stage, which subsequently dictates macroscopic precipitation. The presence of frustrated clusters and the local enthalpy minimization explains the unusual (meta)stability, slow dynamics, and gelatinous crystallization behaviors of supersaturated sodium aluminate solution. On the other hand, the emergence of cation−anion prenucleation clusters in potassium aluminate solutions promotes liquid−liquid separation events, which are responsible for fast diffusion dynamics and the rapid onset of nucleation. More generally, the intimate roles that counterions and water solvents play in determining the bonding dynamics and potential effects on the preferential stabilization of specific molecular complexes or polymeric species, while most evident at high salt concentrations, are likely ubiquitous throughout solution chemistry. This concept can be further tested by the molecular simulations and transition state theory to quantify the local coordination state of molecular species that are stable and perhaps dominating the overall reaction dynamics in solution. We close by reiterating that the identity of countercations controls the local specific interactions responsible for distinct solvent−solute clustering dynamics in concentrated solutions and demonstrates the potential to use ion-specific effects to promote greener, more energy-efficient aluminum processing technologies as well as chemical strategies for the control of crystallization processes beyond the classical settings.

■ ASSOCIATED CONTENT

Supporting Information

The Supporting Information is available free of charge on the ACS Publications website at DOI: 10.1021/acs.jpclett.9b01416.

(1) Experimental details of the alkaline aluminate solution preparation and solution composition summarized in Table S1, (2) QENS experimental methods and data fitting analyses, (3) ^{1}H PFG-NMR and ^{27}Al NMR experimental details and results, (4) details on Raman spectroscopy measurements, and (5) descriptions on the complementary neutron diffraction analyses for the deuterated-equivalent aluminate solutions (PDF)

■ AUTHOR INFORMATION

Corresponding Author

*E-mail: wangh3@ornl.gov.

ORCID

Hsiu-Wen Wang: 0000-0002-2802-4122
Trent R. Graham: 0000-0001-8907-8004
Eugene Mamontov: 0000-0002-5684-2675
Katharine Page: 0000-0002-9071-3383
Andrew G. Stack: 0000-0003-4355-3679
Carolyn I. Pearce: 0000-0003-3098-1615

Notes

The authors declare no competing financial interest.

■ ACKNOWLEDGMENTS

This research was supported by IDREAM (Interfacial Dynamics in Radioactive Environments and Materials), an Energy Research Center funded by the U.S. Department of Energy (DOE), Office of Science, Basic Energy Sciences (BES). NMR was performed using facilities at the Environmental Molecular Science Laboratory (EMSL), a national scientific user facility sponsored by the DOE Office of Biological and Environmental Research (BER) at Pacific Northwest National Laboratory (PNNL). PNNL is a multi-program national laboratory operated for DOE by Battelle Memorial Institute operating under Contract No. DE-AC05-76RL0-1830. Research at the BASIS and NOMAD beamlines at Spallation Neutron Source (SNS), Oak Ridge National Laboratory (ORNL) were sponsored by the Scientific User Facilities Division, BES, DOE. QClimax software is made available through ICE-MAN: Integrated Computational Environment, Modeling and Analysis of Neutron data (LDRD 8237) project, funded by the Laboratory Directed Research and Development program at ORNL.

DOI: 10.1021/acs.jpclett.9b01416
J. Phys. Chem. Lett. XXXX, XXX, XXX−XXX

REFERENCES

(1) Suo, L.; Borodin, O.; Gao, T.; Olguin, M.; Ho, J.; Fan, X.; Luo, C.; Wang, C.; Xu, K. "Water-in-Salt" Electrolyte Enables High-Voltage Aqueous Lithium-Ion Chemistries. *Science* **2015**, *350*, 938−943.

(2) Genovese, D.; Montalti, M.; Otalora, F.; Gomez-Morales, J.; Sancho-Tomas, M.; Falini, G.; Garcia-Ruiz, J. M. Role of $CaCO_3$ Degrees Neutral Pair in Calcium Carbonate Crystallization. *Cryst. Growth Des.* **2016**, *16*, 4173−4177.

(3) Jin, G. B.; Lin, J.; Estes, S. L.; Skanthakumar, S.; Soderholm, L. Influence of Countercation Hydration Enthalpies on the Formation of Molecular Complexes: A Thorium-Nitrate Example. *J. Am. Chem. Soc.* **2017**, *139*, 18003−18008.

(4) Reichenbach, J.; Wynne, K. Frustration Vs Prenucleation: Understanding the Surprising Stability of Supersaturated Sodium Thiosulfate Solutions. *J. Phys. Chem. B* **2018**, *122*, 7590−7596.

(5) Rao, A.; Cölfen, H. From Solute, Fluidic and Particulate Precursors to Complex Organizations of Matter. *Chem. Rec.* **2018**, *18*, 1203.

(6) Henzler, K.; Fetisov, E. O.; Galib, M.; Baer, M. D.; Legg, B. A.; Borca, C.; Xto, J. M.; Pin, S.; Fulton, J. L.; Schenter, G. K.; Govind, N.; Siepmann, J. I.; Mundy, C. J.; Huthwelker, T.; De Yoreo, J. J. Supersaturated Calcium Carbonate Solutions Are Classical. *Sci. Adv.* **2018**, *4*, No. eaao6283.

(7) Habraken, W. J.; Tao, J.; Brylka, L. J.; Friedrich, H.; Bertinetti, L.; Schenk, A. S.; Verch, A.; Dmitrovic, V.; Bomans, P. H.; Frederik, P. M.; Laven, J.; van der Schoot, P.; Aichmayer, B.; de With, G.; DeYoreo, J. J.; Sommerdijk, N. A. Ion-Association Complexes Unite Classical and Non-Classical Theories for the Biomimetic Nucleation of Calcium Phosphate. *Nat. Commun.* **2013**, *4*, 1507.

(8) Gebauer, D.; Raiteri, P.; Gale, J. D.; Cölfen, H. On Classical and Non-Classical Views on Nucleation. *Am. J. Sci.* **2018**, *318*, 969−988.

(9) Gebauer, D.; Kellermeier, M.; Gale, J. D.; Bergstrom, L.; Cölfen, H. Pre-Nucleation Clusters as Solute Precursors in Crystallisation. *Chem. Soc. Rev.* **2014**, *43*, 2348−2371.

(10) Sebastiani, F.; Wolf, S. L.; Born, B.; Luong, T. Q.; Cölfen, H.; Gebauer, D.; Havenith, M. Water Dynamics from Thz Spectroscopy Reveal the Locus of a Liquid-Liquid Binodal Limit in Aqueous $Caco_3$ Solutions. *Angew. Chem., Int. Ed.* **2017**, *56*, 490−495.

(11) Widmer, D. R.; Schwartz, B. J. Solvents Can Control Solute Molecular Identity. *Nat. Chem.* **2018**, *10*, 910−916.

(12) Kellermeier, M.; Picker, A.; Kempter, A.; Cölfen, H.; Gebauer, D. A Straightforward Treatment of Activity in Aqueous $CaCO_3$ Solutions and the Consequences for Nucleation Theory. *Adv. Mater.* **2014**, *26*, 752−757.

(13) Drexler, C. I.; Miller, T. C.; Rogers, B. A.; Li, Y. C.; Daly, C. A., Jr.; Yang, T.; Corcelli, S. A.; Cremer, P. S. Counter Cations Affect Transport in Aqueous Hydroxide Solutions with Ion Specificity. *J. Am. Chem. Soc.* **2019**, *141*, 6930−6936.

(14) Gebauer, D.; Wolf, S. E. Designing Solid Materials from Their Solute State: A Shift in Paradigms toward a Holistic Approach in Functional Materials Chemistry. *J. Am. Chem. Soc.* **2019**, *141*, 4490−4504.

(15) Collins, K. D. Ions from the Hofmeister Series and Osmolytes: Effects on Proteins in Solution and in the Crystallization Process. *Methods* **2004**, *34*, 300−311.

(16) Collins, K. D.; Neilson, G. W.; Enderby, J. E. Ions in Water: Characterizing the Forces That Control Chemical Processes and Biological Structure. *Biophys. Chem.* **2007**, *128*, 95−104.

(17) Jenkins, H. D. B.; Marcus, Y. Viscosity B-Coefficients of Ions in Solution. *Chem. Rev.* **1995**, *95*, 2695−2724.

(18) Corridoni, T.; Mancinelli, R.; Ricci, M. A.; Bruni, F. Viscosity of Aqueous Solutions and Local Microscopic Structure. *J. Phys. Chem. B* **2011**, *115*, 14008−14013.

(19) Qvist, J.; Schober, H.; Halle, B. Structural Dynamics of Supercooled Water from Quasielastic Neutron Scattering and Molecular Simulations. *J. Chem. Phys.* **2011**, *134*, 144508.

(20) Russo, J.; Tanaka, H. Understanding Water's Anomalies with Locally Favoured Structures. *Nat. Commun.* **2014**, *5*, 3556.

(21) Zhu, F.; Hirata, A.; Liu, P.; Song, S.; Tian, Y.; Han, J.; Fujita, T.; Chen, M. Correlation between Local Structure Order and Spatial Heterogeneity in a Metallic Glass. *Phys. Rev. Lett.* **2017**, *119*, 215501.

(22) Turton, D. A.; Hunger, J.; Hefter, G.; Buchner, R.; Wynne, K. Glasslike Behavior in Aqueous Electrolyte Solutions. *J. Chem. Phys.* **2008**, *128*, 161102.

(23) Kobayashi, M.; Tanaka, H. Possible Link of the V-Shaped Phase Diagram to the Glass-Forming Ability and Fragility in a Water-Salt Mixture. *Phys. Rev. Lett.* **2011**, *106*, 125703.

(24) Sipos, P. The Structure of Al(III) in Strongly Alkaline Aluminate Solutions - A Review. *J. Mol. Liq.* **2009**, *146*, 1−14.

(25) Johnston, C. T.; Agnew, S. F.; Schoonover, J. R.; Kenney, J. W.; Page, B.; Osborn, J.; Corbin, R. Raman Study of Aluminum Speciation in Simulated Alkaline Nuclear Waste. *Environ. Sci. Technol.* **2002**, *36*, 2451−2458.

(26) Clark, S. B.; Buchanan, M.; Wilmarth, B. *Basic Research Needs for Environmental Management*; Pacific Northwest National Lab (PNNL): Richland, WA, 2016.

(27) Casey, W. H. Large Aqueous Aluminum Hydroxide Molecules. *Chem. Rev.* **2006**, *106*, 1−16.

(28) Wesolowski, D. J. Aluminum Speciation and Equilibria in Aqueous Solution: I. The Solubility of Gibbsite in the System Na-K-Cl-OH-$Al(OH)_4$ from 0 to 100 °C. *Geochim. Cosmochim. Acta* **1992**, *56*, 1065−1091.

(29) Tobler, D. J.; Stawski, T. M.; Benning, L. G. Silica and Alumina Nanophases: Natural Processes and Industrial Applications. In *New Perspectives on Mineral Nucleation and Growth*; 2017; pp 293−316.

(30) Li, J.; Prestidge, C. A.; Addai-Mensah, J. The Influence of Alkali Metal Ions on Homogeneous Nucleation of $Al(OH)_3$ Crystals from Supersaturated Caustic Aluminate Solutions. *J. Colloid Interface Sci.* **2000**, *224*, 317−324.

(31) Wildman, A.; Martinez-Baez, E.; Fulton, J.; Schenter, G.; Pearce, C.; Clark, A. E.; Li, X. Anticorrelated Contributions to Pre-Edge Features of Aluminate Near-Edge X-Ray Absorption Spectroscopy in Concentrated Electrolytes. *J. Phys. Chem. Lett.* **2018**, *9*, 2444−2449.

(32) Addai-Mensah, J.; Li, J.; Prestidge, C. A. Aggregation Behaviour of Gibbsite Crystals in Supersaturated Sodium and Potassium Aluminate Liquors. *Dev. Chem. Eng. Miner. Process.* **2002**, *10*, 539−551.

(33) Kaduk, J. A.; Pei, S. The Crystal Structure of Hydrated Sodium Aluminate, $NaAlO_2{\cdot}5/4H_2O$, and Its Dehydration Product. *J. Solid State Chem.* **1995**, *115*, 126−139.

(34) Weinberger, M.; Schneider, M.; Zabel, V.; Müller, D.; Gessner, W. Nonanatrium-Bis (Hexahydroxoaluminat)-Trihydroxid-Hexahydrat ($Na_9[Al(OH)_6]_2(OH)_3{\cdot}6H_2O$) - Kristallstruktur, Nmr-Spektroskopie Und Thermisches Verhalten. *Z. Anorg. Allg. Chem.* **1996**, *622*, 1799−1805.

(35) Qiu, G.; Chen, N. Phase Study of the System Na_2O-Al_2O_3-H_2O. *Can. Metall. Q.* **1997**, *36*, 111−114.

(36) Du, C.; Zheng, S.; Zhang, Y. Phase Equilibria in the K_2O-Al_2O_3-H_2O System at 40 °C. *Fluid Phase Equilib.* **2005**, *238*, 239−241.

(37) Cao, S.; Zhang, Y.; Zhang, Y. Nucleation and Morphology of Monosodium Aluminate Hydrate from Concentrated Sodium Aluminate Solutions. *Cryst. Growth Des.* **2010**, *10*, 1605−1610.

(38) Grishchenko, R. O.; Emelina, A. L. Synthesis and Thermochemical Characteristics of $Na_2O{\cdot}Al_2O_3{\cdot}2.5H_2O$. *Russ. J. Phys. Chem. A* **2013**, *87*, 1−5.

(39) Graham, T. R.; Semrouni, D.; Mamontov, E.; Ramirez-Cuesta, A. J.; Page, K.; Clark, A.; Schenter, G. K.; Pearce, C. I.; Stack, A. G.; Wang, H. W. Coupled Multimodal Dynamics of Hydrogen-Containing Ion Networks in Water-Deficient, Sodium Hydroxide-Aluminate Solutions. *J. Phys. Chem. B* **2018**, *122*, 12097−12106.

(40) Li, J.; Prestidge, C. A.; Addai-Mensah, J. Viscosity, Density, and Refractive Index of Aqueous Sodium and Potassium Aluminate Solutions. *J. Chem. Eng. Data* **2000**, *45*, 665−671.

DOI: 10.1021/acs.jpclett.9b01416
J. Phys. Chem. Lett. XXXX, XXX, XXX−XXX

(41) Sipos, P.; Stanley, A.; Bevis, S.; Hefter, G.; May, P. M. Viscosities and Densities of Concentrated Aqueous NaOH/NaAl(OH)$_4$ Mixtures at 25 °C. *J. Chem. Eng. Data* **2001**, *46*, 657−661.
(42) Sipos, P. M.; Hefter, G.; May, P. M. Viscosities and Densities of Highly Concentrated Aqueous MOH Solutions (M^+ = Na^+, K^+, Li^+, Cs^+,$(CH_3)_4N^+$) at 25.0 °C. *J. Chem. Eng. Data* **2000**, *45*, 613−617.
(43) Singwi, K. S.; Sjolander, A. Resonance Absorption of Nuclear Gamma-Rays and the Dynamics of Atomic Motions. *Phys. Rev.* **1960**, *120*, 1093−1102.
(44) Teixeira, J.; Bellissent-Funel, M. C.; Chen, S. H.; Dianoux, A. J. Experimental Determination of the Nature of Diffusive Motions of Water Molecules at Low Temperatures. *Phys. Rev. A: At., Mol., Opt. Phys.* **1985**, *31*, 1913−1917.
(45) Holz, M.; Heil, S. R.; Sacco, A. Temperature-Dependent Self-Diffusion Coefficients of Water and Six Selected Molecular Liquids for Calibration in Accurate ^{1}H NMR PFG Measurements. *Phys. Chem. Chem. Phys.* **2000**, *2*, 4740−4742.
(46) Mamontov, E. Diffusion in Confinement as a Microscopic Relaxation Mechanism in Glass-Forming Liquids. *Chem. Phys. Lett.* **2012**, *530*, 55−60.
(47) Ben Ishai, P.; Mamontov, E.; Nickels, J. D.; Sokolov, A. P. Influence of Ions on Water Diffusion - A Neutron Scattering Study. *J. Phys. Chem. B* **2013**, *117*, 7724−7728.
(48) Graham, T. R.; Han, K. S.; Dembowski, M.; Krzysko, A. J.; Zhang, X.; Hu, J.; Clark, S. B.; Clark, A. E.; Schenter, G. K.; Pearce, C. I.; Rosso, K. M. ^{27}Al Pulsed Field Gradient, Diffusion-Nmr Spectroscopy of Solvation Dynamics and Ion Pairing in Alkaline Aluminate Solutions. *J. Phys. Chem. B* **2018**, *122*, 10907−10912.
(49) Hess, B.; van der Vegt, N. F. Cation Specific Binding with Protein Surface Charges. *Proc. Natl. Acad. Sci. U. S. A.* **2009**, *106*, 13296−13300.
(50) Chen, B.; Ivanov, I.; Park, J. M.; Parrinello, M.; Klein, M. L. Solvation Structure and Mobility Mechanism of OH^-: A Car-Parrinello Molecular Dynamics Investigation of Alkaline Solutions. *J. Phys. Chem. B* **2002**, *106*, 12006−12016.
(51) Semrouni, D.; Wang, H.-W.; Clark, S. B.; Pearce, C. I.; Page, K.; Schenter, G.; Wesolowski, D. J.; Stack, A. G.; Clark, A. E. Resolving Local Configurational Contributions to X-Ray and Neutron Radial Distribution Functions within Solutions of Concentrated Electrolytes - A Case Study of Concentrated NaOH. *Phys. Chem. Chem. Phys.* **2019**, *21*, 6828−6838.
(52) Hellström, M.; Behler, J. Structure of Aqueous NaOH Solutions: Insights from Neural-Network-Based Molecular Dynamics Simulations. *Phys. Chem. Chem. Phys.* **2017**, *19*, 82−96.
(53) Tossell, J. A. Theoretical Studies on Aluminate and Sodium Aluminate Species in Models for Aqueous Solution: $Al(OH)_3$, $Al(OH)_4^-$, and $NaAl(OH)_4$. *Am. Mineral.* **1999**, *84*, 1641−1649.
(54) Gale, J. D.; Rohl, A. L.; Watling, H. R.; Parkinson, G. M. Theoretical Investigation of the Nature of Aluminum-Containing Species Present in Alkaline Solution. *J. Phys. Chem. B* **1998**, *102*, 10372−10382.
(55) Pouvreau, M.; Dembowski, M.; Clark, S. B.; Reynolds, J. G.; Rosso, K. M.; Schenter, G. K.; Pearce, C. I.; Clark, A. E. Ab Initio Molecular Dynamics Reveal Spectroscopic Siblings and Ion Pairing as New Challenges for Elucidating Pre-Nucleation Aluminum Speciation. *J. Phys. Chem. B* **2018**, *122*, 7394−7402.
(56) Yu, X. Y.; Yao, J.; Lao, D. B.; Heldebrant, D. J.; Zhu, Z.; Malhotra, D.; Nguyen, M. T.; Glezakou, V. A.; Rousseau, R. Mesoscopic Structure Facilitates Rapid CO_2 Transport and Reactivity in CO_2 Capture Solvents. *J. Phys. Chem. Lett.* **2018**, *9*, 5765−5771.
(57) Gebauer, D.; Volkel, A.; Cölfen, H. Stable Prenucleation Calcium Carbonate Clusters. *Science* **2008**, *322*, 1819−1822.
(58) Wallace, A. F.; Hedges, L. O.; Fernandez-Martinez, A.; Raiteri, P.; Gale, J. D.; Waychunas, G. A.; Whitelam, S.; Banfield, J. F.; De Yoreo, J. J. Microscopic Evidence for Liquid-Liquid Separation in Supersaturated $CaCO_3$ Solutions. *Science* **2013**, *341*, 885−889.
(59) Johansson, G. The Crystal Structure of the Potassium Aluminate $K_2[Al_2O(OH)_6]$. *Acta Chem. Scand.* **1966**, *20*, 15.

DOI: 10.1021/acs.jpclett.9b01416
J. Phys. Chem. Lett. XXXX, XXX, XXX−XXX